Scientific
Research

Influence of Oxygen to Argon Ratio on the Structural and Morphological Properties of Nb-Doped SrTiO₃ Epitaxial Films Grown by Reactive Ion Beam Sputter Deposition

Gasidit Panomsuwan[1], Nagahiro Saito[1,2,3]

[1]Department of Materials, Physics and Energy Engineering, Graduate School of Engineering, Nagoya, Japan
[2]EcoTopia Science Institute, Nagoya University, Nagoya, Japan
[3]Green Mobility Collaborative Research Center, Nagoya, Japan
Email: gasidit@rd.numse.nagoya-u.ac.jp

ABSTRACT

Nb-doped SrTiO₃ (STNO) films were grown on (001)-oriented LaAlO₃ substrates by a reactive ion beam sputter deposition at various $O_2/(Ar+O_2)$ mixing ratios (OMRs) with a substrate temperature of 800°C. The STNO films exhibited good crystallinity with an epitaxial orientation as characterized by high-resolution X-ray diffraction, grazing-incidence X-ray diffraction, and in-plane pole figure analysis. A decrease of out-of-plane and in-plane lattice constants was observed with an increase of OMR. The surface morphology of the STNO films showed a very dense fine-grain structure. The root-mean-square roughness was found to be increased as the OMR increased. Moreover, the elemental compositions of the STNO films were examined by X-ray photoelectron spectroscopy.

Keywords: Nb-Doped SrTiO₃; Epitaxial Films; Crystal Structure; Ion Beam Sputter Deposition.

1. Introduction

SrTiO₃ (STO) has received much attention in the past decade as a potential material for a wide range of electronic devices owing to its excellent dielectric properties [1-3]. Another interesting property of STO is the ability to adjust the electrical conductivity, which is achievable with an n-type semiconductor and metallic behaviors by doping an appropriate level of impurity atoms (e.g. La^{2+}, Nb^{5+}, etc.) [4,5]. Very recently, n-type semiconductor Nb-doped STO (STNO) has become an attractive material for thermoelectric applications, and has also served as the bottom electrodes for perovskite ferroelectric thin-film capacitors [6,7]. Most studies extensively used pulsed laser deposition (PLD) and molecular beam epitaxy (MBE) to grow the epitaxial STNO films with control at an atomic level. However, they are not suitable for large area deposition in the viewpoint of industrial processes. Electron-cyclotron-resonance ion beam sputter deposition (ECR-IBSD) has been demonstrated as a potential technique for fabricating complex oxide films with high crystalline quality and flat surface. It also provides several advantages, such as well-controlled ion energy and growth rate, low operating pressure, (~5 × 10⁻⁵ - 5 × 10⁻⁴ Torr), good film adhesion, and ease of fab-

rication of thin film over a large area [8,9]. The ECR ion source is a non-filament type, leading to a long lifetime and allowing for the use of various kinds of gas species [10]. Not only selecting a suitable growth technique, but the effect of growth conditions on the physical properties of the film is also very important to consider. Oxygen pressure has been found to be a critical parameter for the growth of oxide films because it significantly affects the crystal structure, surface morphology, stoichiometry, and electrical properties [11-14]. Therefore, careful control of the oxygen pressure during growth is very important in order to obtain films with desirable properties.

In the present study, we have focused on the growth of epitaxial STNO films using the reactive ECR-IBSD technique. The effects of the $O_2/(Ar+O_2)$ mixing ratio (OMR) to their structural and morphological properties were studied and discussed.

2. Experimental

STNO films were grown on (001)-oriented LaAlO₃ (LAO) single crystal substrates using the ECR-IBSD technique. 20 mol% Nb-doped STO was used as a target. To prepare the substrate with atomically flat surface, the LAO substrates (MTI Corporation) were ultrasonically

cleaned with acetone and ethanol (purity 99.0%, Wako Pure Chemical Industries) followed with etching in concentrated hydrochloric acid (37 wt%, Sigma-Aldrich) under ultrasonic agitation at room temperature [15]. The chamber was initially evacuated to a base pressure of $<2 \times 10^{-6}$ Torr. The cleaned LAO substrates were placed above the target in parallel at a distance of 40 mm. The STNO films were grown on the LAO substrates at various OMRs (12.5%, 25.0%, 37.5% and 50.0%), while total pressure of the Ar + O_2 gas mixtures was maintained at 6×10^{-4} Torr. These were the optimal condition to obtain the stable beam during film growth. The gas mixtures were discharged by a microwave ECR ion source $(f = 2.45\,\text{GHz})$ at a fixed power output of 180 W. Then the ions were extracted from the source at a voltage of 1800 V and delivered to the target at an incident angle of 45˚. All films were grown at a substrate temperature of 800˚C.

Structural properties of the STNO films were characterized by x-ray diffraction (XRD, Rigaku SmartLab) with CuK_α radiation (λ = 1.5418 Å). The X-ray power was 9 kW. Surface morphology of the films was observed by atomic force microscopy (AFM, Seiko Instrument, SPA-300HV). To analyze elemental composition, X-ray photoelectron spectroscopy (XPS) measurement was performed with an Omicron ESCA Probe (Omicron, Nanotechnology). Monochromatic MgK_α radiation (photon energy of 1256.6 eV) was used as an excitation source.

3. Results and Discussion

3.1. Structural Properties

Figure 1 shows a grazing-incidence X-ray reflection (GIXRR) spectrum of the STNO film grown on the LAO substrate. The oscillation pattern began to be observed at an angle greater than the critical angle $(\alpha_C \approx 0.315˚)$. The film thickness could be determined from the period of this oscillation. The inset of **Figure 1** demonstrates average growth rate as a function of OMR. By increasing OMR, the average growth rate decreased from 0.56 to 0.17 nm/min due to its low sputtering yield. This growth rate was calculated by dividing the film thickness (as extracted from GIXRR) by the growth time. A high-resolution X-ray diffraction (HRXRD) $\omega-2\theta$ scan in **Figure 2(a)** revealed only 00*l* reflection peaks corresponding to the STNO film and the LAO substrate without the reflection peaks from randomly oriented grains and impurity phases, such as with Nb_2O_3, $SrNb_2O_7$, $SrNb_2O_6$ or Nb_2TiO_7. This indicated that the STNO films were single phase, and preferred (001) orientation in a direction normal to the substrate surface. A grazing incidence x-ray diffraction (GIXRD) $2\theta\chi$ scan was also measured and shown in **Figure 2(b)**. An incident angle was fixed at
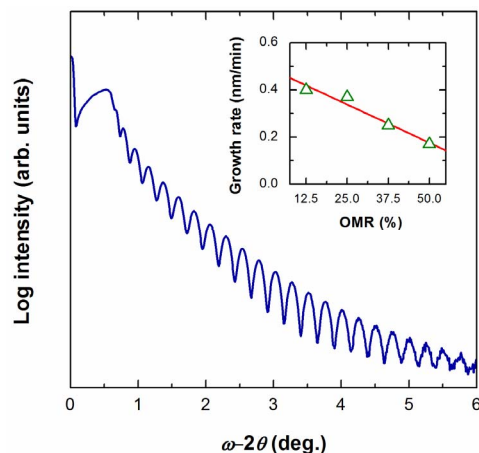

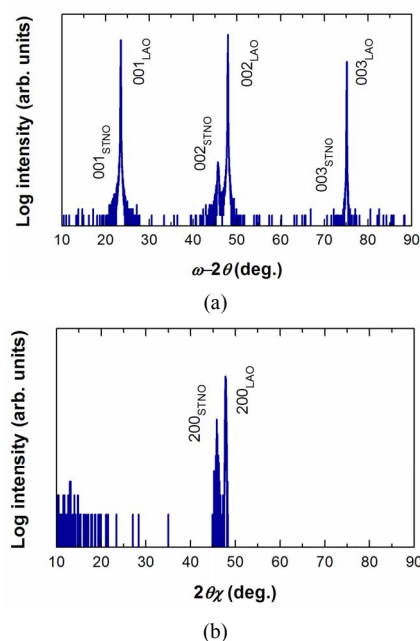**Figure 1. GIXRR spectrum of the STNO film grown on LAO substrate. The inset shows growth rate as a function of OMR.**

Figure 2. (a) HRXRD $\omega-2\theta$ scan and (b) GIXRD $2\theta\chi$ scan of the STNO film grown on LAO substrate at 25% OMR.

ω = 0.3˚ for the measurement, which provided the penetration depth near the film surface. The measurement was fixed at a scattering vector normal to the 200_{LAO} plane. Only the 200_{STNO} peak together with the 200_{LAO} peak along the $2\theta\chi$ scan was detected, indicating good in-plane alignment. The same HRXRD and GIXRD patterns were found for all STNO films.

Figures 3(a) and **(b)** present the HRXRD $\omega-2\theta$ scans and GIXRD $2\theta\chi$ scans around the 002_{STNO} and 200_{STNO} reflections, respectively. Pendellösung fringes were clearly seen around the 002_{STNO} reflection from the HRXRD spectra, which provided evidence that the grown films had good crystallinity, smooth surfaces, and

well-defined film/substrate interfaces. Another observation was a slight shift of the 002_{STNO} and 200_{STNO} reflections toward a higher angle, suggesting a change of the crystal lattice structure. Out-of-plane and in-plane lattice constants calculated from the angle position of the 002_{STNO} and 200_{STNO} reflections, respectively, using Bragg's law were plotted as a function of OMR in **Figure 4**. The out-of-plane lattice constants were larger than in-plane lattice constants for all films. This implied that the STNO films grew on the LAO substrate with a tetragonal structure due to an in-plane compressive stress from the LAO substrate. With an increase of OMR, both out-of-plane and in-plane lattice constants decreased, while tetragonality (c/a) increased from 1.001 to 1.003. The larger lattice constants at low OMR were attributed to Ti^{3+} and Nb^{4+} ions induced by oxygen vacancies. The ion radii of Ti^{3+} (67 pm) and Nb^{4+} (68 pm) are much larger than those of Ti^{4+} (60.5 pm) and Nb^{5+} ions (64 pm), resulting in lattice expansion [16].
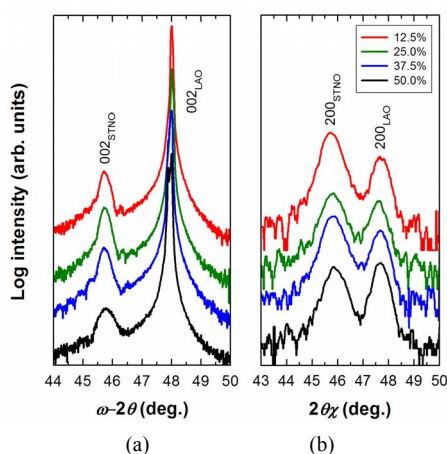

Figure 3. (a) HRXRD $\omega-2\theta$ scans around 002_{STNO}; and (b) GIXRD $2\theta\chi$ scans around the 200_{STNO} reflections of the STNO films grown at various OMRs.

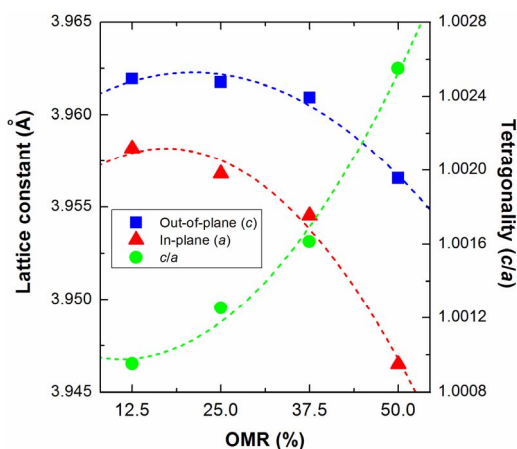Orientation quality of the STNO films was confirmed by out-of-plane and in-plane rocking curve measurements on the 002_{STNO} reflection (ω scan) and the 200_{STNO} reflection (ϕ scan), respectively. The out-of-plane rocking curve consisted of two intensity components: a narrow peak corresponding to the reflection from a good alignment of crystal, and a broad peak corresponding to local atomic displacement. This behavior is normally found in epitaxial layers due to the presence of misfit dislocations lying at the film/substrate interface. Full-width at half-maximum (FWHM) of the out-of-plane rocking curve was found to be the lowest value for the film grown at 25% OMR, which was about 0.1° and 1° for the narrow and broad peaks, respectively. A gradual increase of the FWHM of out-of-plane rocking curve was investigated when the OMR was greater than 25%. This suggested that the orientation quality of the films dropped when they grew at over 25% OMR. On the other hand, in-plane rocking curve revealed only one peak with the FWHM of about 1° and remained almost constant with increasing OMR. The FWHMs of out-of-plane and in-plane rocking curves plotted versus the OMR are shown in **Figure 5**.

To confirm in-plane orientation of the STNO films on the LAO substrates, an in-plane pole figure analysis was examined on the $\{011\}_{LAO}$ and $\{011\}_{STNO}$ planes by fixing the 2θ at ~33.4° and ~32.2°, respectively. By varying $\beta\left(0 < \beta < 360°\right)$ and $\alpha\left(0 < \alpha < 90°\right)$, the samples were rotated relative to the scattering vector. Both in-plane pole figures revealed four intense spots at $\alpha \approx 45°$ with an equal space of 90° at the same β-angle position $\left(\beta = 0°, 90°, 180°\text{ and }270°\right)$, as depicted in **Figure 6**. This result confirmed that the films exhibited a cube-on-cube orientation and a good in-plane alignment. The orientation relationship could be given as:

$$(001)_{STNO}\left\|(001)_{LAO}\right. \quad \text{and} \quad [110]_{STNO}\left\|[110]_{LAO}\right.$$

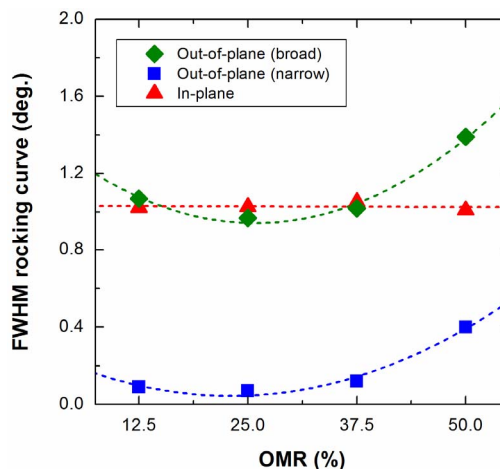**Figure 4. Lattice constants and tetragonality (c/a) of the STNO films as a function of OMR.**

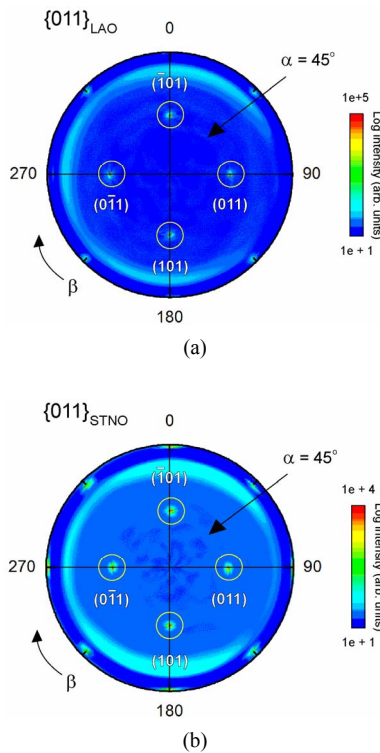**Figure 5. FWHMs of out-of-plane and in-plane rocking curves of the STNO films grown at various OMRs.**

Figure 6. In-plane pole figures measured on (a) the $\{011\}_{LAO}$ and (b) the $\{011\}_{STNO}$ planes.

3.2. Surface Morphology

AFM topography images of the STNO film surfaces grown at various OMRs are illustrated in **Figure 7**. Three-dimensional islands covered on the substrate terrace were clearly observed. Moreover, the film surfaces became rougher as the OMR increased. The rms roughness was increased up to about 0.32 nm when the OMR reached 50%. This might be attributed to the different physical and chemical properties of the vapor species. At higher OMR, these species lost their kinetic energy due to the scattering effect of oxygen molecules, leading to a decrease of surface mobility and lateral growth inhibition.

3.3. Elemental Composition Analysis

All binding energies detected with XPS wide scans showed that the STNO films were composed of Sr, Ti, Nb, and O elements. Elemental compositions near the film surface were obtained by quantitative analysis using Sr3d, Ti3p, Nb3d, and O1s peaks. It was found that the compositional ratio of $Sr/(Ti+Nb)$ was close to unity. **Figure 8** shows a narrow scan of O1s, which consisted of two overlapping peaks. One peak at a lower binding energy $\left(E_B \approx 530\,\text{eV}\right)$ was attributed to the lattice oxygen $\left(O_L\right)$ in the film. Another peak at a higher binding energy $\left(E_B \approx 532\,\text{eV}\right)$ arose from the chemically adsorbed oxygen on the film surface $\left(O_C\right)$. The peak of
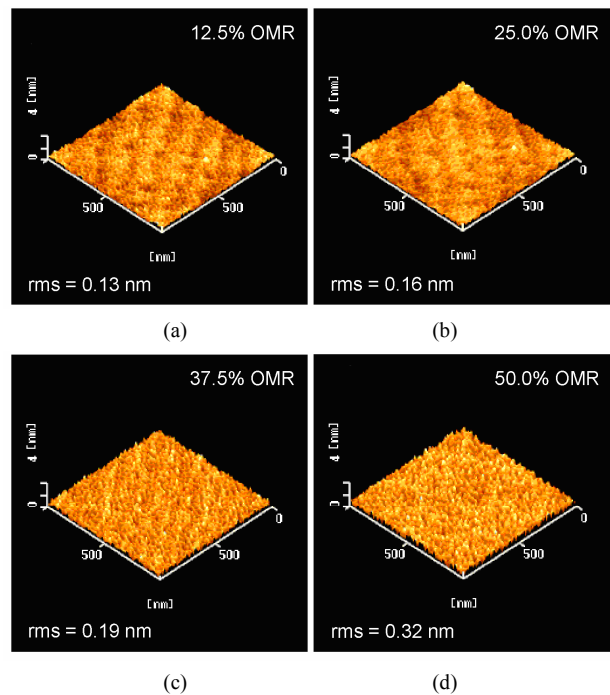

Figure 7. AFM topography images ($1 \times 1\ \mu m^2$ scan area) of the STNO films grown at various OMRs: (a) 12.5%; (b) 25.0%; (c) 37.5%; and (d) 50.0%.
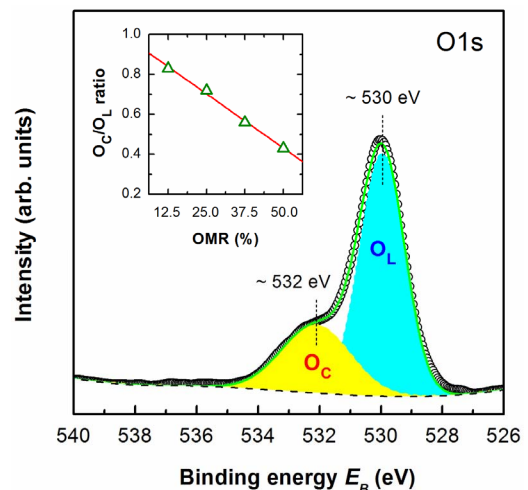

Figure 8. Narrow scan XPS spectrum of the O1s peak of STNO film. The inset shows the relative ratio of O_C/O_L as a function of OMR.

chemically adsorbed oxygen was much weaker than that of lattice oxygen in the XPS spectrum. The relative ratio of O_C/O_L calculated from peak areas was found to decrease with an increase of OMR, as demonstrated in the inset of **Figure 8**. A decrease of O_C indicated that oxygen vacancies decreased when the films were grown at higher OMR. This might be explained that there were only a few atoms on the film surface that allowed for the chemical adsorption of oxygen.

4. Conclusion

STNO films were epitaxially grown on the LAO substrates by reactive ECR-IBSD at various OMRs. The OMR was found to significantly influence the growth rate, crystal structure and film quality. Moreover, the rms surface roughness of the films became rougher when the OMR increased. The present study showed that an optimum value for the growth of STNO thin films with good crystallinity and a relatively smooth surface was at 25% OMR. The XPS result showed that the ratio of O_L/O_C was also related to the OMR. We expect that the ECR-IBSD can be a capable method for fabricating high quality films in the research and development of production technology. The obtained results are also useful for selecting optimum growth conditions for further experiments.

5. Acknowledgements

REFERENCES

[1] C. W. Schneider, R. Schneider and H. Rietschel, "High Dielectric Constant and Tunability of Epitaxial $SrTiO_3$ Thin Film Capacitors," *Journal of Applied Physics*, Vol. 85, No. 10, 1999, pp. 7362-7369. doi:10.1063/1.369363

[2] K. Eisenbeiser, J. M. Finder, Z. Yu, J. Ramdani, J. A. Curless, J. A. Hallmark, R. Droopad, W. J. Ooms, L. Salem, S. Bradshaw and C. D. Overgaard, "Field Effect Transistors with $SrTiO_3$ Gate Dielectric on Si," *Applied Physics Letters*, Vol. 76, No. 10, 2000, pp, 1324-1326.

[3] J. Robertson, "High Dielectric Constant Gate Oxides for Metal Oxide Si Transistors," *Reports on Progress in Physics*, Vol. 69, No. 2, 2006, pp. 327-396. doi:10.1088/0034-4885/69/2/R02

[4] T. Tomio, H. Miki, H. Tabata, T. Kawai and S. Kawai, "Control of Electrical Conductivity in Laser Deposited $SrTiO_3$ Thin Films with Nb Doping," *Journal of Applied Physics*, Vol. 76, No. 10, 1994, pp. 5886-5890. doi:10.1063/1.358404

[5] D. Olaya, F. Pan, C. T. Roger and J. C. Price, "Electrical Properties of La-Doped Strontium Titanate Thin Films," *Applied Physics Letters*, Vol. 80, No. 16, 2002, pp. 2928-2930. doi:10.1063/1.1470694

[6] S. Y. Wang, B. L. Cheng, C. Wang, S. Y. Dai, H. B. Lu, Y. L. Zhou, Z. H. Chen and G. Z. Yang, "Reduction of Leakage Current by Co Doping in $Pt/Ba_{0.5}Sr_{0.5}TiO_3/Nb–SrTiO_3$ Capacitor," *Applied Physics Letters*, Vol. 84, 2004, pp. 4116-4118. doi:10.1063/1.1755421

[7] S. Ohta, T. Nomura, H. Ohta, M. Hirano, H. Hosono and K. Koumoto, "Large Thermoelectric Performance of Heavily Nb-Doped $SrTiO_3$ Epitaxial Film at High Temperature," *Applied Physics Letters*, Vol. 87, No. 9, 2005, Article ID: 092108.

[8] A. Biswas, A. K. Poswal, R. B. Tokas and D. Bhattacharyya, "Characterization of Ion Beam Sputter Deposited W and Si Flms and W/Si Interfaces by Grazing Incidence X-Ray Reflectivity, Atomic Force Microscopy and Spectroscopic Ellipsometry," *Applied Surface Science*, Vol. 254, No. 11, 2008, pp. 3347-3356. doi:10.1016/j.apsusc.2007.11.025

[9] G. Panomsuwan, O. Takai and N. Saito, "Fabrication and Characterization of Epitaxial $SrTiO_3$/Nb-Doped $SrTiO_3$ Superlattices by Double ECR Ion Beam Sputter Deposition," *Vacuum*, Vol. 89, 2013, pp. 35-39. doi:10.1016/j.vacuum.2012.08.011

[10] N. Sakudo, K. Tokiguchi, H. Koike and I. Kanomata, "Microwave Ion Source," *Review of Scientific Instruments*, Vol. 48, No. 7, 1977, pp. 462-466. doi:10.1063/1.1135144

[11] K. Fukushima and S. Shibagaki, "Nb Doped $SrTiO_3$ Thin Films Deposited by Pulsed Laser Ablation," *Thin Solid Films*, Vol. 315, No. 1-2, 1998, pp. 238-243. doi:10.1016/S0040-6090(97)00752-9

[12] E. J. Tarsa, E. A. Hachfeld, F. T. Quinlan and J. S. Speck, "Growth-Related Stress and Surface Morphology in Homoepitaxial $SrTiO_3$ Films," *Applied Physics Letters*, Vol. 68, No. 4, 1996, pp. 490-492. doi:10.1063/1.116376

[13] H. L. Cai, X. S. Wu and J. Gao, "Effect of Oxygen Content on Structural and Transport Properties in $SrTiO_{3-x}$ Thin Films," *Chemical Physics Letters*, Vol. 467, No. 4-6, 2009, pp. 313-317. doi:10.1016/j.cplett.2008.11.071

[14] R. Reshmi, M. K. Jayaraj and M. T. Sebastian, "Influence of Oxygen to Argon Ratio on the Properties of RF Magnetron Sputtered $Ba_{0.7}Sr_{0.3}TiO_3$ Thin Films," *Journal of the Electrochemical Society*, Vol. 158, No. 5, 2011, pp. G124-G127. doi:10.1149/1.3566094

[15] T. Ohnishi, K. Takahashi, M. Nakamura, M. Kawasaki, M. Yoshimoto and H. Koinuma, "A-Site Layer Terminated Perovskite Substrate: $NdGaO_3$," *Applied Physics Letters*, Vol. 74, No. 17, 1999, pp. 2531-2533. doi:10.1063/1.123888

[16] W. Martienssen and H. Warlimont, "Springer Handbook of Condensed Matter and Materials Data," Springer, Berlin, 2005.